Letters

EMI Generation Characteristics of SiC and Si Diodes: Influence of Reverse-Recovery Characteristics

Xibo Yuan, Sam Walder, and Niall Oswald

***Abstract*—Silicon carbide (SiC) Schottky diodes with zero reverse-recovery current (RRC) are perceived as superior due to their reduced switching losses. The absence of reverse-recovery behavior in these devices is also expected to result in reduced electromagnetic interference (EMI), compared with the conventional silicon (Si) PIN diodes. In this letter, the influence of SiC Schottky diodes on EMI generation in hard-switched power converters is investigated. A simplified analytical model enabling the spectral envelope of the diode current waveform to be predicted is presented. Numerical simulations and experimental tests are employed to validate this model. It is found that although the reverse-recovery characteristics are very different between Si diodes and SiC Schottky diodes, the actual improvement with SiC diodes on the spectral content of the diode current waveforms is relatively small except at frequencies around 5 MHz. Factors affecting the EMI performance such as the peak amplitude and the "snappiness" of the RRC are also analyzed. Experimental measurements of the switching current waveforms for both Si diodes and SiC diodes are presented and their frequency spectra are compared.**

***Index Terms*—Electromagnetic interference (EMI), Schottky diode, slicon carbide, reverse recovery.**

I. Introduction

THE ability of power devices based on wide-bandgap semiconductor materials—in particular silicon carbide (SiC) and gallium nitride (GaN)—to deliver significant performance advantages over current silicon-based power devices is well reported [1]–[3]. The properties of these materials allow the fabrication of unipolar devices at much higher voltage ratings than is practical in silicon, resulting in a significantly improved tradeoff between switching and conduction losses. Combined with the higher operating temperature capability and greater thermal conductivity of these materials, these advantages can be exploited to develop power converters with higher power density than is possible with silicon-based devices [2]–[3].

The most commercially mature wide-bandgap power device is the SiC Schottky barrier diode (SBD), which eliminates the reverse-recovery behavior of Si PIN diodes, resulting in very low switching losses. At the time of writing, SiC SBDs are commercially available at voltage ratings up to 3.3 kV, whereas Si SBDs are practically limited by reverse leakage to ratings of less than 200 V [1], [2].

Manuscript received May 10, 2014; revised June 22, 2014; accepted July 5, 2014. Date of publication July 18, 2014; date of current version October 15, 2014. Recommended for publication by Associate Editor H. Chung.

The authors are with the Electrical Energy Management Group, Department of Electrical and Electronic Engineering, the University of Bristol, Bristol BS8 1UB, U.K. (e-mail: xibo.yuan@bristol.ac.uk; sam.walder.2010@my.bristol.ac.uk; niall.oswald@bristol.ac.uk).

Color versions of one or more of the figures in this paper are available online at http://ieeexplore.ieee.org.

Digital Object Identifier 10.1109/TPEL.2014.2340404

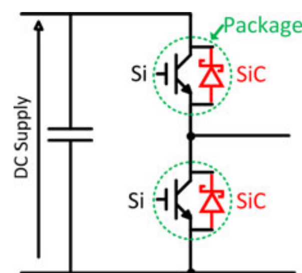

Fig. 1. Half-bridge circuit employing Si IGBTs and SiC SBDs.

In addition to being a significant source of switching losses, diode reverse-recovery behavior is widely recognized as a cause of electromagnetic interference (EMI) generation in hard-switched power converters [4]. It may therefore be expected that replacing Si diodes with SiC SBDs will result in reduced EMI generation due to the absence of reverse-recovery behavior [3]–[6]. Apart from the diode reverse-recovery behavior, the switching operation of other devices (e.g., insulated-gate bipolar transistors (IGBTs), MOSFETs) and their associated switching voltage and current (d*v*/d*t* and d*i*/d*t*) are the main sources of the EMI. The EMI is also highly dependent on the circuit parameters such as parasitic inductance, capacitance, etc. In order to separate the impact of various components on EMI performance, it would be sensible to analyze EMI from the source, e.g., investigation of the spectrum of the diode reverse-recovery current (RRC), which can be a good indicator for the EMI impact of the Si and SiC diodes [7], [8].

SiC diodes are primarily employed in "hybrid" combinations with Si switching devices—e.g., superjunction MOSFETs in power factor correction stages or IGBTs in inverter applications. In the latter case, SiC diodes are located in antiparallel with IGBTs, in both high power modules and "copackaged" as discrete devices for use at lower power levels [9]. Fig. 1 shows the elementary half-bridge circuit comprising Si IGBTs and SiC diodes which is considered in this study. Fig. 2 shows experimental current waveforms of a Si and a SiC diode, where the Si diode has much higher RRC than the SiC diode.

This letter aims to reveal the influence on EMI generation of the elimination of RRC obtained by substituting the conventional Si diodes with SiC diodes in a hard-switched power

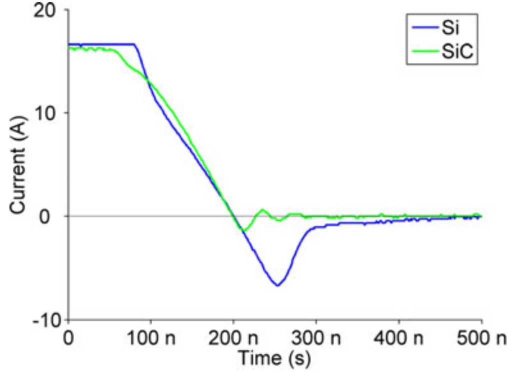

Fig. 2. Current waveforms of a Si PIN diode and a SiC SBD: Si diode (IXDH20N120D1), SiC diode (GA35XCP12-247), dc voltage 52 V, junction temperature 25 °C.

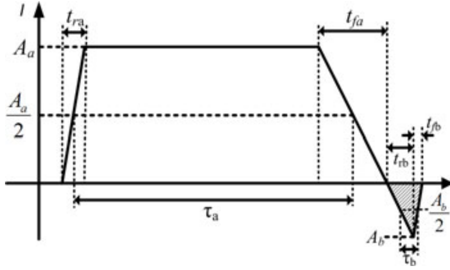

Fig. 3. Simplified approximation of a typical diode current waveform.

converter circuit. A simplified analytical model enabling the spectral envelope of the diode current waveform to be predicted is presented. The key parameters of the diode reverse-recovery characteristics, which affect the harmonic spectrum, have been identified and analyzed. Numerical simulation and experimental tests are employed to validate this model and compare the EMI performance of Si and SiC diodes.

II. Analytical Modeling of Diode Current Waveforms

In EMI analysis, the upper bound or "spectral envelope" of the EMI emissions of a power converter, as opposed to the amplitudes of individual harmonic components, is of most interest to a designer. Simplified analytical models of switching waveforms allow the influence of time-domain waveform parameters on the resulting frequency spectrum to be readily established. In order to perform this analysis, the diode current is approximated by the waveform shown in Fig. 3, where the unhatched trapezoid is the diode forward current, while the hatched triangular area represents the contribution of reverse recovery.

Each segment is characterized by its amplitude (A), its rise and fall times (t_r and t_f), and the pulse width τ (defined between the mid-points of the rising and falling edges). Parameters associated with the trapezoidal and triangular segments are referred to subscripts *a* and *b,* respectively. Note that the triangular portion is taken to be a special case of the trapezoid without the flat top. For the SiC diode, although the RRC is removed, there

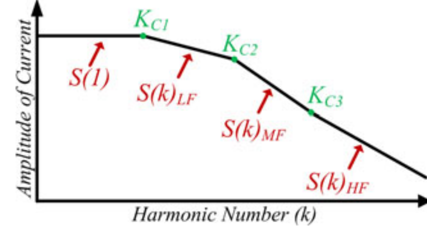

Fig. 4. Analytical spectral envelope parameters.

is a triangular segment due to the charging of the diode junction capacitance.

For a periodic trapezoidal waveform, the spectral envelope in the frequency domain can be described by the parameters shown in Fig. 4 with highlighted cutoff frequencies (K_{C1}, K_{C2}, and K_{C3}) and amplitude of each segment (S(1), $S(k)_{\rm LF}$, $S(k)_{\rm MF}$, and $S(k)_{\rm HF}$). The expressions for these parameters are given in (1)–(7). The spectrum of the waveform in Fig. 3 (including both the forward current and reverse recovery) can then be derived by considering it as two separate trapezoids and summing the spectrum of each [10], [11].

The three cutoff frequencies (K_{C1}, K_{C2}, and K_{C3}) in Fig. 4 are described by

$$K_{c1} = \frac{2}{\frac{\pi}{A} S(1)} \tag{1}$$

$$K_{c2} = \frac{1}{\pi\alpha} \tag{2}$$

$$K_{c3} = \frac{1}{\pi\beta}. \tag{3}$$

The amplitude of the line segments in the corresponding frequency ranges is then described by

$$S(1) = \frac{A}{\pi}\sqrt{\begin{array}{l}(\mathrm{sinc}(\pi R) + \mathrm{sinc}(\pi F))^2 \sin^2(\pi d)\\ + (\mathrm{sinc}(\pi R) - \mathrm{sinc}(\pi F))^2 \cos^2(\pi d)\end{array}} \tag{4}$$

$$S(k)_{\rm LF} = \frac{2A}{\pi k} \tag{5}$$

$$S(k)_{\rm MF} = \frac{A}{\pi k}\left(1 + \frac{1}{\pi k \alpha}\right) \tag{6}$$

$$S(k)_{\rm HF} = \frac{A}{\pi^2 k^2}\left(\frac{1}{R} + \frac{1}{F}\right). \tag{7}$$

Equations (8)–(10) define the derived parameters used in (1)–(7)

$$R = \frac{t_r}{T},\ F = \frac{t_f}{T},\ d = \frac{\tau}{T} \tag{8}$$

$$\alpha = \mathrm{MAX}(R, F),\ \beta = \mathrm{MIN}(R, F) \tag{9}$$

$$f = k f_0. \tag{10}$$

In (10), f is the harmonic frequency and f_0 is the fundamental (switching) frequency, which is 20 kHz in all cases considered

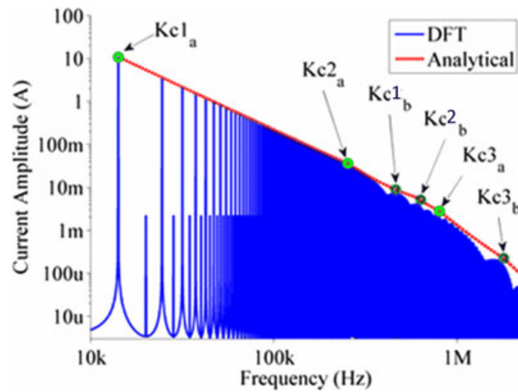

Fig. 5. Comparison of numerical and analytical methods.

here. k represents the harmonic order[10], [11]. With this model, the envelope of the diode current spectrum can be described analytically using a small number of waveform parameters as given in Fig. 3. This in turn allows the investigation of the differences in spectral characteristics that would arise if a SiC diode was used to replace a Si diode, or the effects of varying degrees of the characteristics in either type of diodes.

To demonstrate this method, a hypothetical scenario is examined where the amplitudes of the waveforms are $A_a = 17$ A, $A_b = 7$ A, with rise and fall times $t_{r_a} = 5$ ns, $t_{r_b} = 1$ ns, $t_{f_a} = 50$ ns, and $t_{f_b} = 1$ ns. Then, $\tau_a = 25$ μs and $\tau_b = 8$ ns with the periods of both waveforms being $T = 50$ μs. A simulated waveform corresponding to these parameters is synthesized for 100 cycles and its frequency spectrum computed using the discrete Fourier transform (DFT) is plotted in Fig. 5 along with the envelope predicted by the analytical model. As seen, the analytical model given in (1)–(7) can accurately predict the spectral envelope of the simulated results with DFT, which validates the effectiveness of the analytical model.

There are two important factors in the diode RRC that can affect the harmonic spectra of the diode current. The first one is the "snappiness" of the diode, which represents how fast the RRC falls back to zero. This "snappiness" is characterized by the parameter t_{fb} in the analytical model given in Fig. 3. Fig. 6(a) shows a range of simulated diode RRC waveforms with different "snappiness," varying from 1 to 30 ns. Fig. 6(b) shows the spectra plots obtained by the DFT of these waveforms. As seen, the amplitude of the high frequency (e.g., >50 MHz) spectral components (EMI) increases with the increase of the diode snappiness (decrease of t_{fb}). However, the difference is only significant when the fall time (t_{fb}) of the RRC becomes much shorter (e.g., 1 or 5 ns) than that of other parts of the current waveform. When, for example, the fall time varies between 20 and 30 ns or even longer, the snappiness of the RRC does not make much difference to the overall diode current spectrum. Investigation of the equations of the analytical model shows that the key effect that decreasing t_{fb} to have is pushing the cutoff frequency k_{c3} higher as given in (3). Fig. 6(c) shows how the three cutoff frequencies vary with t_{fb}. As seen, the k_{c3} increases significantly when t_{fb} reduces below 10 ns. However, when t_{fb} is larger than 20 ns, its effect on k_{c3} is relatively small,

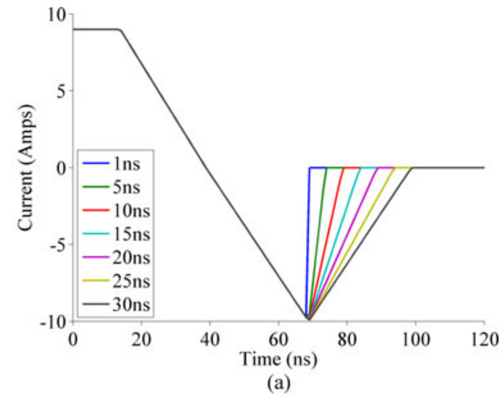

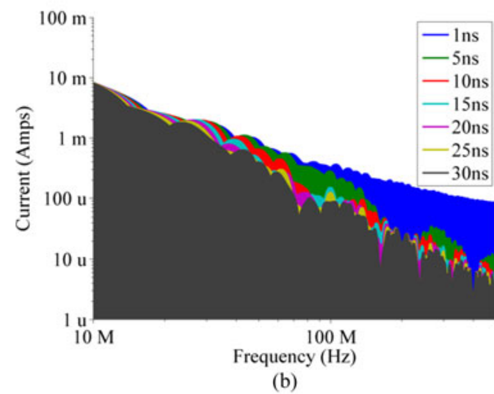

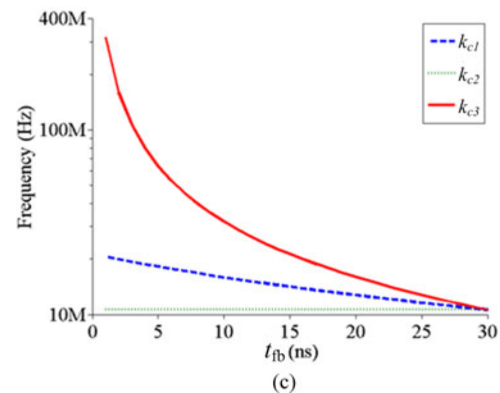

Fig. 6. Impact of diode snappiness (t_{fb}) on the harmonic spectra. (a) Diode current with various snappiness of RRC. (b) DFT results of the diode currents in (a). (c) Variation of cutoff frequencies with t_{fb}.

which agrees with the DFT results shown in Fig. 6(b). This means that if only considering the effect of diode snappiness, replacing a less snappy Si diode (e.g., $t_{fb} > 20$ ns) with a SiC diode would bring little benefits in terms of EMI. It would make more sense to replace a snappy diode with a SiC diode to gain significant EMI reduction from 50 MHz and above.

From the analysis earlier, it can be seen that the steepest slope in the time-domain current determines the high-frequency evolution of the spectrum envelope. Even if some switching transients can be controlled to be soft, the other steeper ones mainly determine the high-frequency tendency. The snap-off of the diode RRC normally cannot be controlled but depends only on the diode technology. Consequently, even if the IGBT

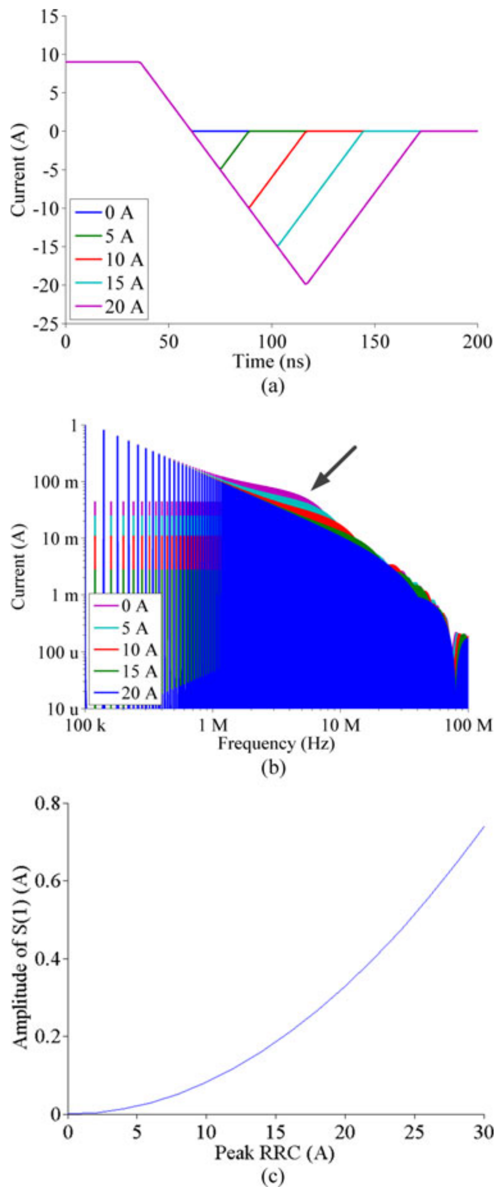

Fig. 7. Impact of the peak amplitude of the diode RRC on the harmonic spectra. (a) Diode current with various peak RRC. (b) DFT results of the diode currents in (a). (c) Variation of the amplitude of $S(1)$ with peak RRC.

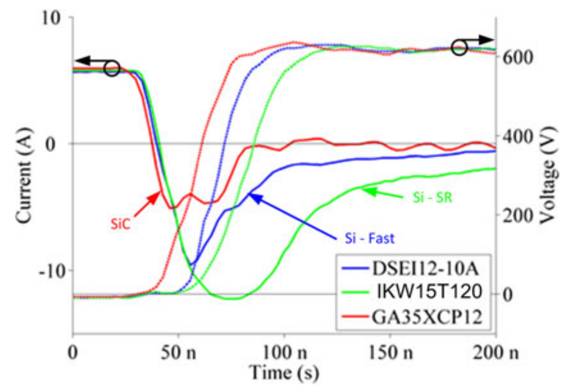

Fig. 8. Diode voltage and current waveforms (Si-fast, Si-SR, and SiC).

or MOSFET switching is controlled (by the gate driver or by snubber circuits) to be soft, the switching cell may be very noisy because of the free recovery of the diode [11]. Therefore, the SiC diode can bring EMI benefit to replace a "snappy" Si diode by removing the RRC.

The second factor affecting the harmonic spectrum is the peak amplitude of the RRC. Fig. 7(a) and (b) illustrates the diode RRC with various amplitude and their DFT results. As seen, when the peak amplitude of the RRC varies from 0 to 20 A in Fig. 7(a), the spectra increase between 1 and 10 MHz as shown in Fig. 7(b). Note that in Fig. 7(a), it is assumed that the reverse-recovery time increases with the amplitude of the RRC and the snappiness of the diode is therefore kept the same. Fig. 7(c) shows how the spectral envelope changes with the peak amplitude of the RRC, which is predicted from the analytical model. As seen, when the peak RRC increases from 0 to 30 A, the amplitude of the first segment of the triangle spectral envelope ($S(1)$) increases from 0 to 0.8 A, which causes the spectra difference shown in Fig. 7(b). Hence, if a Si diode with a high peak RRC is replaced with a SiC diode, the harmonic spectral content (EMI) in certain frequency ranges (e.g., between 1 and 10 MHz) will be reduced.

III. Experimental Test Results

In order to investigate the EMI impact of replacing Si diodes with SiC diodes and validate the predictions made by the analytical models in the previous sections, a selection of diodes was obtained for analysis with the aim of finding a fast diode and a slow soft-recovery (SR) diode to compare with the SiC diode. The current and voltage waveforms for the tested diodes are shown in Fig. 8. All the diodes are tested with a half-bridge configuration given in Fig. 1, where the top device is an IGBT and the bottom device is replaced with different diodes [12]. The dc supply voltage is 600 V and the IGBT and diode voltage ratings are 1200 V except the diode DSEI 12-10A is rated at 1000 V. All the diodes are tested under the same forward current and the IGBT is driven such that the same di/dt (400 A/μs) is achieved for the diodes' current as shown in Fig. 8. In this way, the diodes' reverse-recovery characteristics (e.g., snappiness and amplitude of the RRC) can be particularly examined. The switching frequency is 20 kHz.

In Fig. 8, the SR Si diode (IKW15T120 [13]) has a very smooth and slow response with the highest amplitude of the RRC. The fast Si diode (DSEI12-10A [14]) has a much faster and sharper response. Finally, the SiC diode (GA35XCP12-247 [9]) has the minimum negative current, which is due to the junction capacitance of the diode.

Each of the current waveforms presented in Fig. 8 has been analyzed using both the analytical model in (1)–(7) and DFT. Table I shows the values that were used in each case to calculate the analytical envelope, which was extracted from the current waveforms in Fig. 8. Note that the fall time (t_f) is measured from the peak of the RRC to 20% of the RRC in order to approximate the triangle presented in the analytical model.

TABLE I
DIODE CURRENT PARAMETERS USED IN THE ANALYTICAL MODEL IN FIG. 3

Device Component	All Trapezoid	DSEI12 (Si-fast) Triangle	IKW15T (Si-SR) Triangle	GA35XCP12 (SiC) Triangle
T	50 μs	50 μs	50 μs	50 μs
A	5.70 A	9.60 A	12.2 A	5.00 A
t_r	44.9 ns	16.4 ns	32.7 ns	8.40 ns
t_f	9.30 ns	48.9 ns	56.2 ns	16.3 ns
τ	24.3 μs	37.5 ns	57.7 ns	35.8 ns

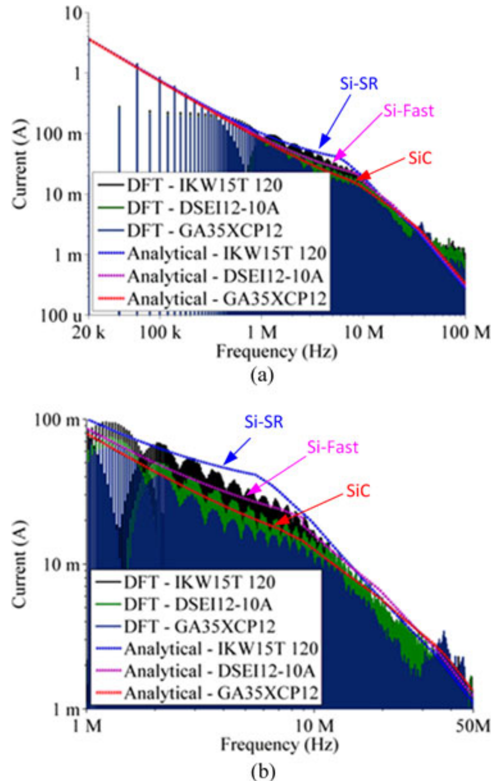

Fig. 9. Current spectra for selected diodes using the analytical model and DFT. (a) 20 kH–100 MHz. (b) Close-up view (1–50 MHz).

Fig. 9(a) shows the analytical spectral envelope and DFT results of the experimental diode current waveforms graphically. As seen, the analytical results agree with the DFT results reasonably well for all the three diodes, which validate the effectiveness of the analytical model.

As seen, though the reverse-recovery characteristics are very different of these three diodes, the spectra difference in the frequency domain (e.g., from 20 kHz to 100 MHz) is actually relatively small. This contradicts the normal thinking that SiC diodes can bring in significant advantage in reducing the EMI by removing the RRC. There are several reasons for this. First, compared with the diode forward current (trapezoid), the RRC (triangle) is relatively a small portion of the total current. Therefore, the impact of the diode RRC characteristics on the total spectrum is limited. Second, although the fast Si diode (DSEI 12-10A) has snappier reverse-recovery characteristics, which is expected to differentiate its spectrum from the spectra of the SiC and the SR Si diode, the actually fall time of the RRC is 48.9 ns (t_f in Table I). As analyzed in Fig. 6, once the fall time is longer than 30 ns, the difference made by the snappiness is very small. Therefore, the snappiness does not make much difference for the spectra of the three diodes. Third, the most observable difference between the spectra is in the frequency range from 1 to 10 MHz, the close-up view of which is shown in Fig. 9(b). The maximum difference between the SR Si diode and SiC diode is around 30 mA (8 dB·mA) at 5 MHz. This difference is due to the fact that the SR Si diode has the highest peak RRC, followed by the fast Si diode and the SiC diode. This agrees with the results explained in Fig. 7.

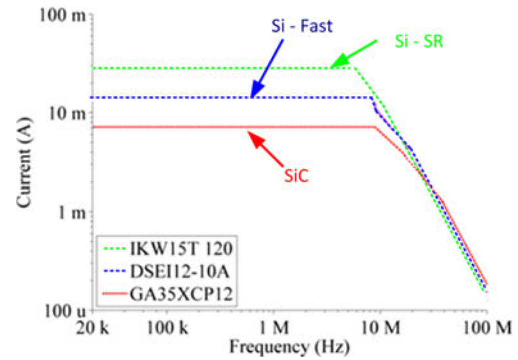

Fig. 10. Spectra contribution of RRC for each of the selected diodes.

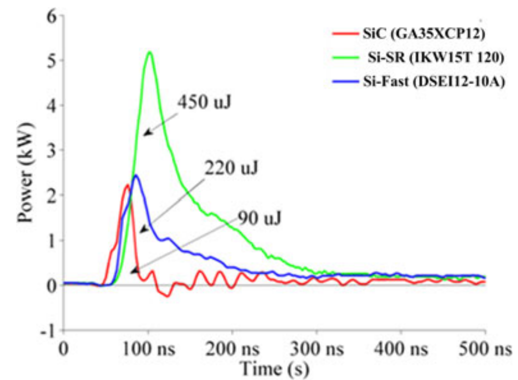

Fig. 11. Reverse-recovery loss for each selected diode.

Fig. 10 further shows the spectra envelope if only the RRC is concerned (no forward current). The spectra differences of these three diodes are mainly in the range between 20 kHz and 10 MHz and are due to the difference of the peak amplitude of the RRC. This spectra difference (due to RRC) added to the spectra of the forward current will give the total spectra as shown in Fig. 9. Fig. 11 additionally shows the reverse-recovery loss generated due to the RRC of the three diodes, which is obtained by multiplying the diode voltage and current. As seen, the SiC diode has the smallest reverse-recovery loss of the three and has clear benefit in reducing the switching losses.

Note that, in the experiment, due to the bandwidth of the current probe, the concerned frequency range is measured up to 100 MHz as shown in Fig. 9(a). The noise floor of the test setup

is around 1 mA across the frequency range, which is observable at 100 MHz in Fig. 9(a). In addition, as noticed in Fig. 9(b), the DFT result of the SiC diode current has a spike around 30–40 MHz. This is due to the ringing observed in the SiC diode current in Fig. 8 as a result of the parastics of the circuit and the snap-off of the current [15]. This EMI spike cannot be predicted by the model in this letter due to the simplification of the diode current waveform with a trapezoidal and a triangular waveform. This phenomenon can however be taken into account by adding the harmonic expression of the ringing on top of the predicted envelop. The resonance (ringing) is circuit dependant and may be mitigated by improved circuit layout design with reduced parasitics. Although the spikes around 30–40 MHz is not desirable, replacing the Si diodes (especially those are snappy and with large RRC) with SiC diodes can reduce the harmonics in other frequency ranges, e.g., between 1 and 10 MHz in Fig. 9(b). Nevertheless, replacing Si diodes with SiC diodes can significantly reduce the switching losses.

IV. Conclusion

This letter has presented an analytical model which can be effectively used to predict the EMI performance of the diode RRC considering various characteristics such as snappiness, peak amplitude, etc. With the analytical model and experimental results, it has been found that the spectra difference between Si and SiC diodes is relatively small except in the frequency range between 1 and 10 MHz due to the amplitude difference of the RRC of the selected diodes. The EMI benefit by replacing the Si diode with SiC diode may be more significant if the Si diode is much snappier (e.g., with a fall time less than 5 ns) and has a much higher amplitude of the RRC. Nevertheless, using the SiC diode can significantly reduce the switching loss of the converter. An EMI spike around 30–40 MHz has also been found with the SiC diode due to ringing caused by the fast snap-off current and the parasitic of the circuit. While this letter mainly focuses on the investigation of the impact of diode RRC on the EMI, the switching characteristics of the main devices (e.g., MOSFETs or IGBTs) will also affect the EMI performance of a switching cell. A further investigation of the interaction of different components of the circuit and their impact on EMI with a conducted and radiated EMI measurement at terminals can be the scope of future work.

References

[1] J. Millan, P. Godignon, X. Perpina, A. Perez-Tomas, and J. Rebollo, “A survey of wide bandgap power semiconductor devices,” *IEEE Trans. Power Electron.*, vol. 29, no. 5, pp. 2155–2163, May 2014.

[2] F. Filsecker, R. Alvarez, and S. Bernet, “The investigation of a 6.5 kW, 1 kA SiC diode module for medium voltage converters,” *IEEE Trans. Power Electron.*, vol. 29, no. 5, pp. 2272–2280, May 2014.

[3] M. O’Neill, “SiC puts new spin on motor drives,” *Power Electron. Technol.*, vol. 31, pp. 2–5, Jan. 2005.

[4] P. Klaus, “Why diode softness matters? Understanding the switching characteristics of fast diodes and their impact on EMI and voltage stress,” in *Proc. Telecommun. Energy Conf.*, vol. 1, Oct. 2013, pp. 162–166.

[5] J. Richmond, “Hard switched silicon IGBT’s? Cut switching losses in half with silicon carbide Schottky diodes,” *Application. Note, CREE*, 2003.

[6] N. Oswald, P. Anthony, N. McNeill, and B. Stark, “An experimental investigation of the trade-off between switching losses and EMI generation with hard-switched all-Si, Si-SiC and all-SiC device combinations,” *IEEE Trans. Power Electron.*, vol. 29, no. 5, pp. 2393–2407, May 2014.

[7] N. Oswald, B. Stark, D. Holliday, W. Drury, and C. Hargis, “Analysis of shaped pulse transitions in power electronic switching waveforms for reduced EMI generation,” *IEEE Trans. Ind. Appl.*, vol. 47, no. 5, pp. 2154–2165, Sep./Oct. 2011.

[8] X. Gong, I. Josifovic, and J. A. Ferreira, “Modeling and reduction of conducted EMI of inverters with SiC JFETs on insulated metal substrate,” *IEEE Trans. Power Electron.*, vol. 28, no. 7, pp. 3138–3146, Jul. 2013.

[9] GeneSiC (2014, Apr.). “Datasheet-GA35XCP12-247,” [Online]. Available: http://www.genesicsemi.com/

[10] A. Nagel and R. W. De Doncker, “Analytical approximations of interference spectra generated by power converters,” in *Proc. IEEE Ind. Appl. Conf.*, vol. 2, Oct. 1997, no. 1, pp. 1564–1570.

[11] F. Costa and D. Magnon, “Graphical analysis of the spectra of EMI sources in power electronics,” *IEEE Trans. Power Electron.*, vol. 20, no. 6, pp. 1491–1498, Nov. 2005.

[12] N. Oswald, B. H. Stark, N. McNeill, and D. Holliday, “High-bandwidth, high-fidelity in-circuit measurement of power electronics switching waveforms for EMI generation analysis,” in *Proc. IEEE Energy Convers. Congr. Expo. Conf.*, Sep. 2011, pp. 3886–3893.

[13] Infineon (2014, Apr.). “Datasheet-IKW15T120,” [Online]. Available: www.infineon.com/dgdl/IKW15T120_Rev2_4G.pdf

[14] IXYS (2014, Apr.). “Datasheet-DSEI 12–10A,” [Online]. Available: http://ixdev.ixys.com/

[15] J. Lutz and R. Baburske, “Some aspects on ruggedness of SiC power devices,” *Microelectron. Rel.*, vol. 54, no. 1, pp. 49–56, Jan. 2014.